RSC Advances

ROYAL SOCIETY OF CHEMISTRY

www.rsc.org/advances

1

Binding Interaction of an Anionic Amino Acid Surfactant with Bovine Serum Albumin: Physicochemical and Spectroscopic investigations combined with Molecular Docking Study

Somnath Dasmandal, Arjama Kundu, Suparna Rudra, and Ambikesh Mahapatra*

Department of Chemistry, Jadavpur University, Kolkata 700 032, India

*Corresponding author. Tel.: +9133 2457 2770 (office), +9133 2432 4586 (residence); fax: +9133 2414 6223.

E-mail addresses amahapatra@chemistry.jdvu.ac.in, ambikeshju@gmail.com

Abstract

The interaction of a synthesised amino acid surfactant, sodium-N-dodecanoylphenylalaninate (AAS) with a transport protein, bovine serum albumin (BSA) has been uncovered employing various physicochemical and spectroscopic techniques like tensiometry, electro kinetic potential measurements, steady-state fluorometry, time-resolved measurements and circular dichroism (CD) at physiological pH and 298 K. The difference in tensiometric responses of AAS in absence and presence of BSA indicates a significant interaction operative between them. The zeta (ξ) potential measurements have been taken into account in assigning the type of binding interaction between them. The steady-state fluorescence study reveals the sequential unfolding of BSA with stepwise adding of AAS. Stern-Volmer and modified Stern-Volmer plots, Scatchard plots and thermodynamic parameters have been employed to find the type of binding of AAS to BSA. The life-time measurements have been carried out to light on the relative amplitude of binding of AAS to the two Trp residues of BSA namely Trp-134 and Trp-213. The changes in protein secondary structure induced by AAS are unveiled by CD measurements. The quantum mechanical calculations involving density functional theory (DFT) and molecular docking analysis have been undertaken in highlighting the interactive phenomenon between the two. Thus this work shows a total inspection on an amino acid surfactant-BSA interaction.

1. Introduction

Proteins are the most important chemical substance in living organisms and take part in almost all biological processes [1]. Serum albumins are the most abundant proteins in blood plasma and the circulatory system, and are responsible for binding of a wide variety of fatty acids, drugs, metal ions and surfactants [2-5]. Interactions of proteins with surfactants have been studied extensively for the past few years due to its numerous applications in biological, industrial, cosmetic and pharmaceutical systems [6-8]. The immense importance of this type of interactive phenomenon lies by virtue of its resemblance with the lipid-protein interaction in the living cell-membrane [9].

Bovine serum albumin (BSA) is a widely known transport protein comprising of 583 amino acid residues in its single polypeptide chain with a molecular mass of 66463 Da [10]. The crystal structure of BSA reveals a heart shaped architecture composed of 17 disulfide bridges and three major domains (I, II and III) each consisting of two sub-domains (A and B). It bears approximately 76% sequence homology with another transport protein, human serum albumin (HSA), and they exhibit a conserved repeating pattern of disulfide linkages [2]. Two Tryptophan (Trp) residues are housed at positions 134 and 213 in the amino acid sequence of BSA among which Trp-134 is somewhat bare [11]. At physiological pH, BSA is negatively charged [10].

Proteins are very much prone to get unfolding upon the action of drug molecules, denaturant and surfactants [12-15]. It has been established that the presence of surfactant not only changes the functional properties of the native protein, but the conformational parameters may also get modified notably [16]. It is well documented that surfactants after binding with proteins may induce either stabilization or denaturation to the protein structure. Protein-surfactant interactions are conspicuously dependent on the features of the surfactants

investigated. Both single-chain cationic [17] and anionic [13] surfactants put forth escalating interests to the recent researchers in this regard. Considerable attentions have also been placed on Gemini surfactants resulting denaturation of BSA structure [18]. Not only single chain surfactants, but twin-chain surfactants may also interact with BSA causing amendment in protein conformation [19]. However, among these surfactants, the interaction between anionic surfactant and protein is of the utmost interest. This is because; the anionic surfactants interact strongly with protein molecules and denature them even at very low concentrations. Thus the anionic surfactants often behave as an efficient denaturant than the common chemical denaturants such as urea, guanidine hydrochloride etc [20]. Surfactants are also known to influence protein aggregation which in many cases leads to perturbation of various biological functions of proteins. These aggregation processes are associated with the formation of cataracts in the lens of the eye, Alzheimer's disease due to aggregation of amyloidogenic proteins and other neurological diseases [21, 22]. Therefore, understanding of the nature of protein-surfactant interaction is seemed to be essential with respect to the advancement of the fields of pharmaceutical and cosmetic research [23]. In this context, one of the most extensively investigated systems is BSA–SDS system [24]. Mukherjee *et al* have recently proposed the sequential unfolding after initial stabilisation of BSA structure upon the addition of sodium dodecyl sulphate (SDS) surfactant [25]. Although a more recent study on the interaction of a twin-chain surfactant, sodium bis-2-ethylhexyl sulfosuccinate (AOT) with BSA suggests that AOT binds to BSA in a different manner from that we observed for SDS−BSA interaction [26]. However, to the best of our knowledge, there is no such investigation reported on the interaction of BSA with anionic biocompatible amino acid surfactant (AAS) bearing carboxylate (–COO⁻) head group and amide linkage in its alkyl chain. Amino acid surfactants are now widely used in pharmaceuticals, food, cosmetic

products and industrial detergency for their low toxicity and quick biodegradability [27].

Thus there is a pressing need in deciphering the mode of binding of AAS with serum protein.
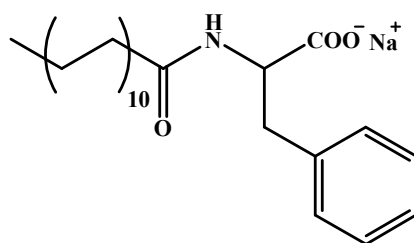
Scheme 1: Structure of amino acid surfactant (AAS)

In our present work, we have used a synthesised amino acid surfactant containing phenylalanine as the amino acid residue. By virtue of its structure, AAS has an amide linkage in between the phenylalanine moiety and hydrophobic alkyl chain (Scheme 1) which may act as both, donor and acceptor of H-bonds. Therefore, it can be anticipated that AAS may interact with BSA through hydrophobic and/or H-bonding and van der Waals forces of interaction. The interactive phenomenon between AAS and BSA has been exploited by surface tension, ξ-potential, fluorescence and circular dichroism measurements. Theoretical support from molecular modelling study has been given for better understanding of the role of molecular structure of AAS in BSA−AAS interaction in stabilising and/or denaturing the BSA structure.

2. Materials and methods

2.1. Materials

Lauric acid, thionyl chloride and phenylalanine have been used as received from SRL, India. All the solvents have been procured from Merck, India and distilled prior to use. Bovine serum albumin, BSA (essentially fatty acid and globulin free) has been procured from Sigma-Aldrich and used as received. All other reagents from Merck, India have been used without further purification. The solutions of BSA and surfactant have been prepared in 10 mM

Britton-Robinson buffer of pH 7.4. The concentration of buffered solution of BSA has been kept at 3.0 μM during the experiments except for circular dichroism study where 0.15 μM BSA solutions have been used as per instrumental requirement. The concentration of BSA solution has been determined each time when required from UV-Vis spectra using $\varepsilon_{280} =$ 43,824 M^{-1} cm^{-1} [28]. Highly pure water from Millipore synergy (India) has been used throughout the experiments.

2.1.1. Synthesis of anionic amino acid surfactant (AAS)

Sodium-N-dodecanoylphenylalaninate (AAS) has been synthesised, purified and recrystallised following the reported procedure [29]. The scheme of synthesis of the surfactant is given in supporting information (Scheme S1). Firstly, dodecanoylchloride has been prepared upon reacting of lauric acid (1.0 g equivalent) with thionyl chloride (1.5 g equivalent) in chloroform. Another precursor i.e., phenylalanine methyl ester hydrochloride has been then prepared from L-phenylalanine, where an amount of 4.5 g (27.0 mmol) of L-phenylalanine is added to an ice cold methanol (50 mL) followed by the addition of 1.4 mmol thionyl chloride ($SOCl_2$). The solution of phenylalanine methyl ester hydrochloride in chloroform has been treated with triethylamine (NEt_3) under ice cold condition. To this mixture, chloroform solution of dodecanoyl chloride has been added drop wise with continuous stirring at room temperature. The so obtained white powdered product *N*-dodecanoyl-L-phenylalanine methyl ester has been dissolved in THF: MeOH (1: 1) mixture which has been then treated with 1 M NaOH solution and subsequent addition of 1 M HCl solution has been carried out. The mixture has been then extracted with ethyl acetate. The solid mass has been then dried and recrystallised from methanol.

2.1.2. Characterisation of *N*-dodecanoyl-L-phenylalanine

<u>NMR data</u>

The synthesised amino acid surfactant has been characterised by ^{1}H NMR analysis and the representative spectrum is given in Fig. S1 (supporting information). ^{1}H NMR (300 MHz, CDCl$_3$); δ (ppm): 0.86−0.90 (3H, t, terminal CH$_3$), 1.24 (16H, bs, (CH$_2$)$_8$), 1.55 (2H, s, CH$_2$ β to CO), 2.15−2.20 (2H, t, CH$_2$ α to CO), 3.09 – 3.28 (2H, m, CH$_2$Ph), 4.83 – 4.89 (1H, q, CH α to NH), 5.94 – 5.96 (1H, d, NH), 7.15 – 7.30 (5H, m, C$_6$H$_5$).

<u>Surface tension measurement</u>

The critical micelle concentration (CMC) of the synthesised surfactant has been determined using du Nouy tensiometer (experimental procedure has been explained in method section). The tensiometric profile of AAS in aqueous medium is given in Fig. S2. The CMC of AAS is found as 0.93 mM which is in good agreement to the reported data [29, 30].

<u>Absorption and emission spectra</u>

The UV-Vis absorption spectrum of AAS in aqueous buffer medium is shown in Fig. S3. The maximum absorption is observed to be positioned at wavelength of 258 nm which resembles to the characteristic peak of phenylalanine (λ_{max} = 257 nm) due to aromatic component in the structure [31]. The surfactant exhibits weak emission upon exciting at wavelength of 258 nm (Fig. S4), and the emission maximum located at wavelength of 282 nm is also the characteristic emission of phenylalanine [31].

Methods

2.2.1. Experimental

Surface tension measurements have been carried out using a calibrated du Nouy tensiometer (Jencon, India) employing ring detachment technique [32]. The measurements have been

performed upon stepwise addition of AAS in absence and presence of buffered BSA (3.0 µM). Each measurement has been repeated at least three times and the reproducibility of the data has been estimated within ± 0.2 mN m^{-1}.

Surface charge of BSA in absence and presence of AAS has been measured by Malvern (UK), Zetasizer Nano ZS90. The average values of triplicate measurements are reported. Solutions have been twice filtered through 0.45 µm membrane filters in order to remove dust and suspended particles from the system.

Steady-state absorption measurements have been carried out using UV-Vis Spectrophotometer (Shimadzu, UV-1800) equipped with a Peltier temperature controller, TCC-240A in order to maintain a constant temperature of 298 K (± 0.1 K). Quartz cells from Hellma (1 cm path length) have been used in this study. The buffer solution has been used as reference. During the optical titration of BSA, an equal amount of AAS has been added to both the sample and reference cells in order to cancel out the contribution of the added surfactant to the absorbance of BSA spectra. The change in absorption at λ_{max} of BSA upon stepwise addition of AAS has been noted until saturation point.

Steady-state fluorescence measurements have been performed on a Shimadzu RF-5000 spectrofluorometer thermostated at 298 K (± 0.1 K). The intrinsic fluorescence of BSA has been examined upon exciting at 295 nm using excitation and emission band slits at 3 nm and 5 nm respectively. The emission of BSA has been monitored in the wavelength range of 305 nm to 450 nm with maximum at 342 nm of the native BSA. However, it is now widely established that while investigating the binding process between protein and a small molecule employing fluorometric technique, 'inner-filter effect' should be eliminated [33]. The 'inner-filter effect' commonly arises if there is any absorption of the molecule added during fluorescence titration at the wavelength of excitation or at the wavelength used to note the

emission, and the results of which is spurious decrease in the observed fluorescence intensity [31]. To eliminate this artifact, we have made a critical look on the UV-Vis spectrum of AAS at the maximum added concentration during fluorescence titration, and shown in Fig. S3. From the Fig. S3, it can be seen that the change in absorbance due to AAS at both the excitation (295 nm) and emission (342 nm) wavelength of BSA is indeed very small. Nevertheless, we have made an effort to measure the impact of inner-filter effect on the observed fluorescence intensity of BSA. Since the geometry of the spectrofluorometer that we have used in our present case is such that the collected intensity comes exactly from the centre of the cuvette. Thus the inner-filter effect has been estimated from the relation [31] (Eq. 1):

$$I_{obs} = I_{corr} \times 10^{-\frac{A_{ex}\, d_{ex}}{2} - \frac{A_{em}\, d_{em}}{2}} \tag{1}$$

where, I_{obs} is the measured fluorescence, I_{corr} is the corrected fluorescence that is in the absence of inner-filter effect, d_{ex} and d_{em} are the path length of the cuvette (in cm) in the direction of excitation and emission light respectively, and A_{ex} and A_{em} are the change in absorbance at the excitation and emission wavelength of BSA respectively resulted by the addition of AAS.

Time-resolved measurements have been performed employing time-correlated single-photon-counting (TCSPC) technique at room temperature (298 K). A nanosecond diode laser at 300 nm (IBH UK) has been used as an excitation source with a TBX photon detector and the signals have been collected at the magic angle of 54.7°. The luminescence decays have been analysed using IBH DAS-6 software. The goodness of fit of decay data has been evaluated from χ^2 data. The average fluorescence life-times ($\langle \tau \rangle$) for bi-exponential iterative fittings have been estimated from the decay times (τ_1 and τ_2) and the normalised pre-exponential factors (a_1 and a_2) from the following relation [31] (Eq. 2):

10

$$\langle \tau \rangle = a_1 \, \tau_1 + a_2 \, \tau_2 \tag{2}$$

Circular dichroism (CD) spectra have been recorded on a JASCO J-815 spectropolarimeter using a rectangular quartz cuvette of 1 cm path length. The reported CD spectra have been obtained employing a scan speed of 50 nm /min and the baseline has been corrected appropriately. All the CD measurements have been carried out at room temperature (298 K). The CD data have been expressed as mean residue ellipticity (MRE) in deg cm^2 $dmol^{-1}$ using the following equation (Eq. 3)

$$MRE = \theta_{obs} \, M / \, nlC \tag{3}$$

where, θ_{obs} is CD in mdeg, M is the molecular weight of BSA in g $dmol^{-1}$, n is the number of amino acid residue in the protein (here it is 583), l is the path length of the cell (1 cm) and C is the concentration of BSA in g L^{-1}.

2.2.2. Theoretical

The crystal structure of BSA used in the docking study has been extracted from the structure (pdb id: 4F5S) available in Protein Data Bank (PDB) [34]. Polar hydrogen atoms and Gasteiger charges have been then added to prepare BSA molecule for docking analysis. For docking of AAS with BSA, the ground state geometry of AAS has been optimised employing density functional theory (DFT) using B3LYP functional with the standard basis set, 6-31G* in Gaussian 09 program suit [35]. The required pdb structure of AAS has been then derived from the optimised structure. AAS has been considered as ligand and BSA as a receptor for the docking study. The molecular docking analysis has been performed applying the Lamarckian Genetic Algorithm (LGA) implemented in AutoDock 4.2 [36]. The BSA has been laid over a three dimensional grid box, the size of which has been set to ($126 \times 126 \times$

126) $Å^3$ along x-, y-, and z-axis with 0.675 Å spacing. The output from AutoDock has been

further analysed using PyMOL software [37].

3. Results and discussion

3.1. Surface tension measurements

Tensiometry proves itself a useful technique that could provide indication of interaction

between protein and surfactants [24-c]. In our present study, the surface tension (γ) of the

buffered surfactant (AAS) solution have been measured in the absence and presence of BSA

(3.0 μM), and the representative plots of γ *versus* log{[AAS]/M} are shown in Fig. 1. In the

absence of BSA, γ decreases linearly with increasing AAS concentration up to a certain

value, above which it remains constant, thereby producing a well-defined break point,

corresponding to the cmc of AAS under buffered condition (Table 1). However, the surface

tension of buffered BSA solution (58.5 mN m^{-1}) is somewhat lower than that of pure buffer

(69.36 mN m^{-1}), indicating feeble surface activity of BSA. The tensiometric profile of AAS

containing BSA (Fig. 1) shows an initial slow diminution of γ up to point C_1 (0.085 mM

AAS), followed by a steep decrease to reach the final plateau at 0.54 mM AAS (C_m)

corresponding to cmc of AAS (Table 1).
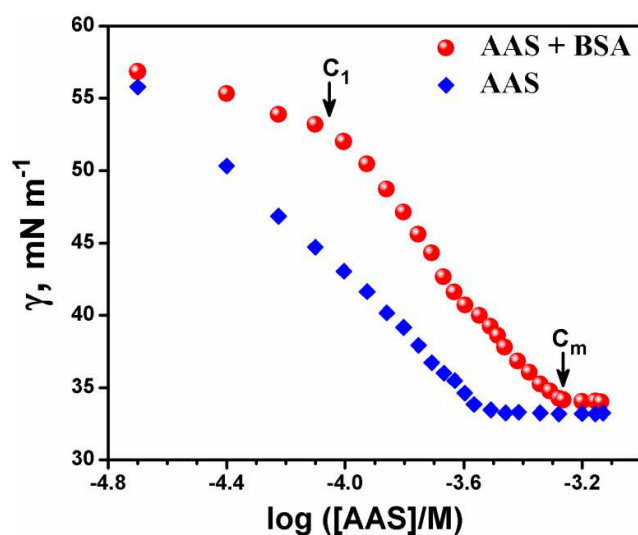
Fig. 1: Variation of surface tension of AAS in the absence and presence of BSA at 298 K, [BSA] = 3.0 μM

The slow diminution of γ up to C_1 is attributed to the monomeric adsorption of AAS onto specific sites of BSA leading to the formation of AAS-BSA (monomer) complex. This complex exhibits less surface activity than pure AAS as evident from the higher γ values of the complex (Fig. 1). Santos *et al* have shown in a classy manner that the complex formed by the monomeric adsorption of SDS onto BSA surface is more surface active than the SDS monomers [38]. While a more recent studies by Mahajan *et al* on the interaction of AOT to BSA, it is found that the resulting AOT-BSA (monomer) complex is less surface active than pure AOT [26]. Hence, the tensiometric profile of AAS, particularly in the low concentration region, is seemed to be quite similar to that for AOT and not like SDS, although both are anionic surfactants. In this region, AAS monomer is seemed to bind with BSA through hydrophobic and/or H-bonding and van der Waals forces of interaction, causing initial unfolding of protein secondary structure. The thermodynamic parameters determined from fluorescence data (discussed later) suggests that the H-bonding interaction via the amide group of AAS and van der Waals forces play an important role in this respect. After C_1, γ decreases more steeply with the addition of AAS up to C_2 indicating stronger interaction between BSA and AAS which in turn implies the formation of highly surface active AAS-BSA complexes. The AAS-BSA complex being negatively charged, repels the BSA (since BSA is negatively charged under the experimental condition) causing it to expand. This in turn exposes more binding sites buried in the core of tertiary structure of BSA [26], thereby allowing AAS to bind to BSA in the form of both monomers and small aggregates. The plateau as observed after C_m indicates the saturation of binding of AAS to BSA and the added AAS results in the formation of free micelles in the bulk. The cmc of AAS in the presence of

BSA is shifted to higher value than that of pure AAS (Table 1). This can be ascribed to the fact that the micellization process is hindered considerably by the monomeric binding of AAS to BSA.

The Gibbs adsorption isotherm is being widely useful to ascertain the interfacial adsorption efficacy of surfactant, which is quantified in terms of maximum surface excess (Γ_{max}) and minimum surface area per surfactant molecule (A_{min}) [39]. These two parameters are indicative of the surface arrangement of surfactant at air/water interface and can be calculated using the following equations (Eq. 4 & 5):

$$\Gamma_{max} = -\frac{1}{n'RT}\left(\frac{\partial \gamma}{\partial \boldsymbol{ln\ C}}\right)_{T} \tag{4}$$

$$A_{min} = \frac{1}{N_A\Gamma_{max}} \tag{5}$$

where, $(\partial \gamma / \partial \ln C)$ is the maximum slope of the plot of γ *versus* log{[surfactant]/M} near the cmc. R, T, C and N_A are the universal gas constant, Kelvin temperature, molar concentration of surfactant (here, AAS) and Avogadro number respectively, and n' is a constant, the value of which is taken as 1 [40]. Here, the contributions of the counterion and the buffer ions have been neglected, since they have no preference toward the interfacial adsorption. The values of Γ_{max} and A_{min} for interfacial adsorption of AAS in the presence and absence of BSA are given in Table 1. The calculated value of Γ_{max} in BSA-AAS systems is lower than that in pure AAS. Conversely, A_{min}, in the presence of BSA, is higher than in the BSA free system. Hence, it can be inferred that the reduced efficacy of AAS to populate the air/water interfacial monolayer in the presence of BSA is indicative of the presence of solubilised BSA-AAS complex at the monolayer [41].

Table 1: Transition concentrations (C_1 & C_m) and interfacial parameters of AAS in the absence and presence of BSA at 298 K, [BSA] = 3.0 μM

System	C_1, mM	C_m (cmc), mM	$10^6 \Gamma_{max}$, mol m^{-2}	A_{min}, Å^2
AAS	—	0.31 ± 0.02	3.75	44.27
AAS-BSA	0.085 ± 0.01	0.54 ± 0.01	3.38	49.01

3.2. ξ-potential measurements

The nature of binding interactions between protein and surfactant are frequently assigned by monitoring the variation of net surface charge of protein at different contents of surfactant [42]. Fig. 2 shows the change of ξ-potential of buffered solution of BSA (pH 7.4) upon successive addition of AAS. The net surface charge of native BSA, at pH 7.4, is found as -16.9 mV which is in agreement to the literature reports [43]. From Fig. 2, it is observed that at lower concentration of AAS, the change in ξ-potential of the protein is only minute. This is certainly due to the similar charge sign of BSA and AAS. As we increase the surfactant concentration, the effective net charge on BSA increases, suggesting the formation of BSA-AAS complex at an expense of conformational change of the protein. This negative ξ-potential value on adsorption of AAS onto protein indicates that the dominant interaction is non-columbic that may be either hydrophobic, hydrogen bonding or van der Waals forces, and whatever be, all of the modes of interaction are seemed to be logical since we are dealing with an anionic surfactant and a negatively charged protein molecule. Prieto *et al* have also reached to a similar conclusion for complexation between HSA and sodium perfluorooctanoate [42]. However, at higher AAS concentration, the system reaches to plateau (Fig. 2). This is ascribed to the fact that at this stage the surfactant start to form micelles and these micelles of AAS do not interact with BSA.
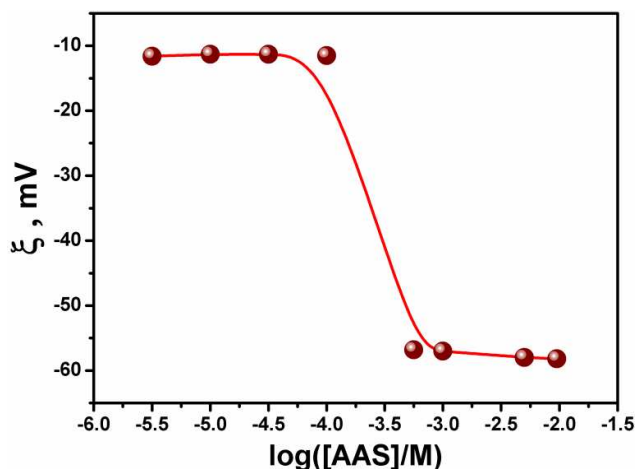
Fig. 2: Influence of AAS concentration on the ξ-potential of buffered BSA solution (pH 7.4) at 298 K, [BSA] = 3.0 µM.

3.3. Intrinsic fluorescence studies

Fluorescence spectroscopy is a widely applied technique in investigating protein conformation, dynamics and intermolecular interactions between surfactants and BSA [44]. The intrinsic fluorescence of BSA depends on three aromatic amino acids *viz.* tryptophan (Trp), tyrosine (Tyr) and phenylalanine (Phe), acting as intrinsic fluorescence probes in this regard. However, Phe is not excited in most of the cases as its quantum yield is quite low, and therefore its emission can be ignored [45]. Hence, the intrinsic fluorescence of BSA is primarily dependent on Trp and Tyr residues [46]. BSA has 18 Tyr residues in its different domains with high abundances in sub domain IC (domain I) and sub domain IIC (domain II). It also possesses two Trp residues, namely Trp-134 and Trp-213. The Trp-134 located in domain I (sub domain IB) lies near the surface of the protein molecule, whereas Trp-213 resides in a hydrophobic cavity of the protein in domain II (sub domain IIA). In this work, the interaction between BSA and AAS has been monitored upon exciting the BSA at 295 nm i.e., Trp excitation (λ_{ex} = 295 nm) has been used to minimise the excitation of Tyr residues and

subsequent hetero-transfer to Trp [47]. Trp emission has been noted in the absence and presence of surfactant throughout the wavelength range of 305 – 450 nm where the emission maximum is found to be centered at 342 nm. The contributions of AAS in the fluorescence spectra of BSA, albeit very small, have been corrected and mentioned in the method section as well (see Fig. S3). A meticulous calculation using Eq. 1 shows that the change in absorbance corresponds to 0.92% (less than 1%) reduction in fluorescence intensity which we have taken into consideration in investigating the binding process between BSA and AAS. Any regular change in the emission intensity (I) as well as maximum emission wavelength (λ_{em}) of BSA from its native state upon the increment of AAS concentration would indicate the micro environmental alteration around the Trp residues The variations of emission spectra of BSA (3.0 µM) at different concentrations of AAS are given in Fig. 3. The inset of Fig. 3 shows the variation of emission maximum (λ_{em}) with concentration of AAS and two distinct breakpoints are observed at 0.058 mM and 0.53 mM which are very close to C_1 and C_m respectively in the tensiometric profile (Fig. 1). The changes in the emission intensity of BSA take place through several distinct phases when subjected to different AAS concentrations (Fig. 3). The emission intensity (I) of BSA initially decreases from its native
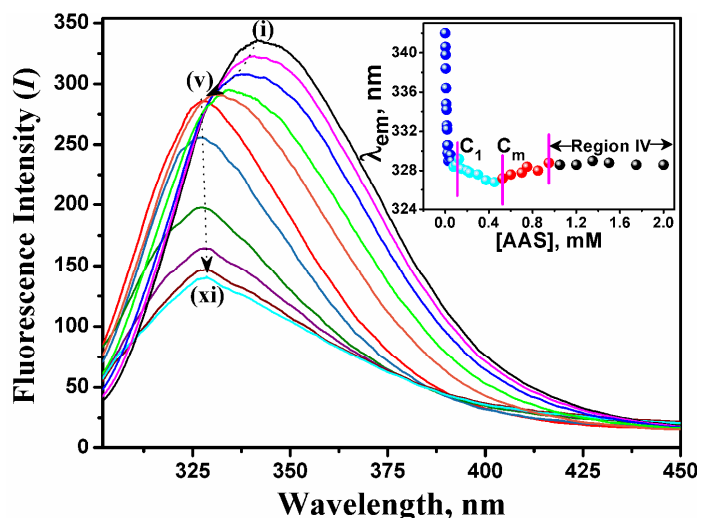
Fig. 3: Intrinsic fluorescence spectra of BSA in the presence of AAS, where (i) → (xi) correspond to 0, 0.0025, 0.005, 0.02, 0.05, 0.2, 0.45, 0.9, 1.05, 1.5 and 2.0 mM AAS at [BSA] = 3.0 μM, 298 K and pH 7.4 Inset: variation of emission maximum (λ_{em}) at various AAS concentration, λ_{ex} = 295 nm.

state up to 0.015 mM AAS (indicated as C_i), beyond which intensity remains almost unchanged over an appreciable range of concentration of AAS, followed by a drastic decrease at higher AAS concentration. It has been shown by Mahajan *et al* that the emission intensity (in terms of normalised area of emission spectra) of BSA increases at low concentration of AOT [26], which indicates that the tendency of AOT to bind to BSA is quite different to that for AAS although both have almost similar tensiometric profile (Fig. 1). It is worth to note here that the perturbation of the absorption spectrum of fluorophore in the presence of ligand suggests the formation of ground state complex between them [48]. Fig. S3 shows that the UV-Vis absorption spectra of BSA and the difference absorption spectra between BSA-AAS and AAS at the same concentration cannot be superimposed within experimental error. The result indicates that the quenching of BSA fluorescence induced by AAS occurs via static quenching mechanism.

3.3.1. Studies on binding and thermodynamic parameters

The binding efficacy of AAS to BSA has been critically analysed employing Stern-Volmer and modified version of Stern-Volmer equations as follows [31, 49]

$$\frac{I_0}{I} = 1 + K_{SV}[Q] \qquad (6)$$

$$\log\left\{\frac{(I_0 - I)}{I}\right\} = \log\left\{\frac{K_a}{M^{-n}}\right\} + n\log\left\{\frac{[Q]}{M}\right\} \qquad (7)$$

where, I_0 and I are emission peak intensities of BSA in the absence and presence of quencher, $[Q]$ is the concentration of the quencher (AAS in our present work). K_{SV} (= $k_q\tau_0$) is Stern-Volmer quenching constant (k_q is the bimolecular quenching constant and τ_0 is the life time of fluorescence in the absence of quencher). The K_a and n are modified Stern-Volmer association constant and the number of binding sites respectively.
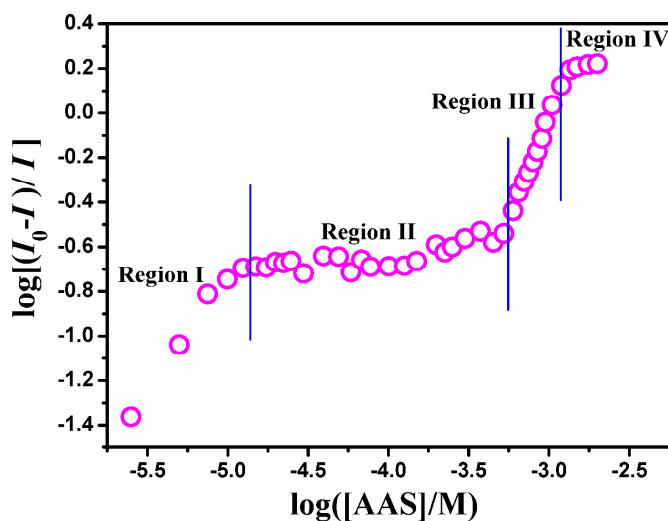
Fig. 4: Plot of log [$(I_0$-I)/I] *versus* log{[AAS]/M} representing various stage of binding of AAS to BSA at [BSA] = 3.0 μM, 298 K and pH = 7.4.

A plot of log[$(I_0$-I)/I] *versus* log{[AAS]/M} is shown in Fig. 4 which indicates that the binding of AAS to BSA takes place in four distinct stages, namely regions I – IV. It is evident

from Fig. 4 that the binding of AAS to BSA is completed at the end of region III i.e. the region IV is a saturation phase. Thus the magnitudes of quenching (K_{SV}) and K_a have been estimated from Stern-Volmer and modified Stern-Volmer plots for the first three regions (Fig. S5 for region I and III) using Eq. 6 & 7 and tabulated in Table S1.

The Fig. 4 suggests that the binding of the surfactant to BSA follows separate mechanisms in various concentration regimes. It is well known that the analyses of Scatchard plots reveal the type of binding of a small ligand molecule to a macromolecular structure, particularly when multi-site ligand binding is suspected [50]. The average number of surfactant molecules bound per BSA molecule (v) can be estimated from fluorescence measurements using the following relation

$$v = \alpha \times C_S/C_P \qquad (8)$$

where α is the fraction of BSA bound to surfactant, C_S and C_P are the total concentration of the surfactant (AAS) and BSA respectively. The values of α have been evaluated from the relation recently used by Mahajan *et al* [26] as

$$\alpha = (A_0 - A)/ (A_0 - A_{min}) \qquad (9)$$

where A denotes the normalised area of emission spectra

The concentration (C_f) of surfactant that remained unbound (i.e., free surfactant) has been calculated from the relation

$$C_f = C_S (1 - \alpha) \qquad (10)$$

Scatchard plot of v/C_f *versus* v as we have obtained is shown in Fig. 5. The concave upward nature of the Scatchard plot is indicative of the existence of negative cooperativity, and non-identical and dependent set of binding sites [51]. Each linear portion of the Scatchard plot has been given a linear fit and from the fitting parameters *i.e.*, slope and intercept, the values of equilibrium binding constant (K) and number of binding sites (n) for that particular region

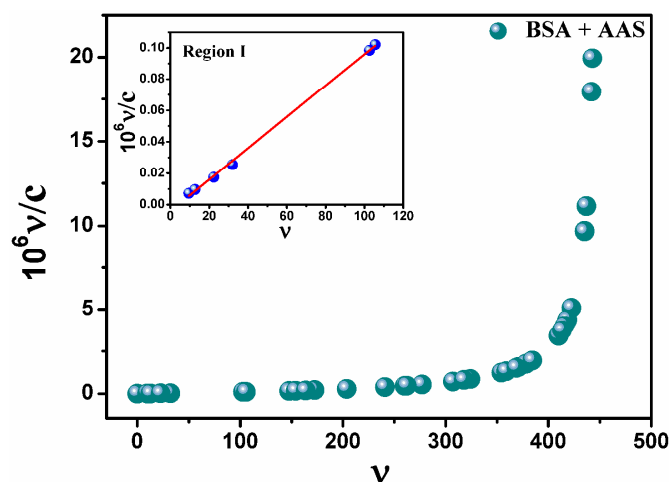(concentration range) have been evaluated [26]. The obtained values of *K* and *n* are represented in Table 2.

Fig. 5. Scatchard plot of BSA with AAS at 298 K, [BSA] = 3.0 μM. Inset: Scatchard plot for region I

In order to highlight the type of interaction between BSA and AAS in different regions, Van't Hoff equation has been employed at three different temperatures

$$\ln K' = -\frac{\Delta H^\circ}{RT} + \frac{\Delta S^\circ}{R} \tag{11}$$

In the present case, K' is analogous to modified Stern-Volmer association constant at the corresponding temperature, ΔH^o and ΔS^o are the standard enthalpy and entropy changes respectively, R is the universal gas constant.

The standard free energy of binding (ΔG_b°) in different regions has been calculated using the following equation (Eq.12)

$$\Delta G_b^\circ = \Delta H^o - T\Delta S^o = -RT \ln K' \tag{12}$$

A good linear relationship between $\ln K'$ versus 1/T is observed at the different regions (Fig. S6 corresponding to region I) assuming that ΔH^o does not undergo considerable change within the investigated temperature range. The values of thermodynamic parameters so obtained are given in Table S2.

In region I, it is observed that λ_{em} shifts from 342 to 329 nm accompanied by a decrease in the emission intensity of BSA upon continuous addition of AAS. The observed blue shift of emission spectra clearly indicates that the fluorophore moves to a less polar environment. From the van't Hoff plot (Fig. S6), the values of ΔH^o and ΔS^o are found as $-36.21(\pm 4.19)$ kJ mol^{-1} and -37.69 (± 1.41) J mol^{-1} respectively signifying that the formation of BSA-AAS complex is primarily an exothermic and enthalpy driven reaction. According to Subramanian *et al* [52], the negative values of ΔH^o and ΔS^o is attributed to the fact that hydrogen bond and van der Waals force play exigent role during the interaction between BSA and AAS. From the Scatchard plot, the values of K and n are found to be very small in this low concentration range (Table 2). In this region, the negative cooperative binding occurs due to the monomeric binding of AAS to a site on the protein with no allosteric effect present to facilitate the additional ligand binding [53]. Thus in the region I, AAS binding is specific in nature, and probably bind near Trp-134 which is somewhat solvent exposed. However, the possibility of binding of AAS to BSA in the vicinity of Trp-213 cannot be ruled out, as the surfactant may insert its hydrophobic tail inside the hydrophobic pocket in sub domain IIA, where Trp-213 is located. The theoretical analysis employing molecular docking study (discussed later) enlightens this binding behaviour of AAS. The amide linkage present in AAS is capable of forming H-bond with the nearby amino acid residues which help in forming the BSA-AAS complex. In this region, the value of quenching constant (K_{SV}) calculated from Stern-Volmer plot (Fig. S5a) is found as 14.8 ($\pm$ 0.5) $\times 10^3$ M^{-1} at 298 K (Table S1). The average life-time of native BSA obtained from life-time measurements (as discussed later) is 5.72 ns. Hence, the

value of k_q comes out as 2.58×10^{12} M^{-1} s^{-1}, which is greater than the largest bimolecular quenching constant in aqueous medium [31]. Hence the progressive decrease in fluorescence intensity of BSA upon the addition of AAS is not an excited state process, but arises out of conformational change in the protein induced by the surfactant binding i.e. static quenching as stated previously. From Stern-Volmer plots at different temperatures (Fig. 6), the K_{SV} values in region I of BSA-AAS system have been calculated and given in Table S2. The data show that K_{SV} decreases with increasing the temperature, conforming that the probable quenching is initiated by ground state complex formation. The amendment in protein conformation in the low concentration region of AAS is also evident from the change in CD spectra as discussed below. The ΔG_b° value (Table S2) indicates that the binding interaction between AAS and BSA is spontaneous in region I.
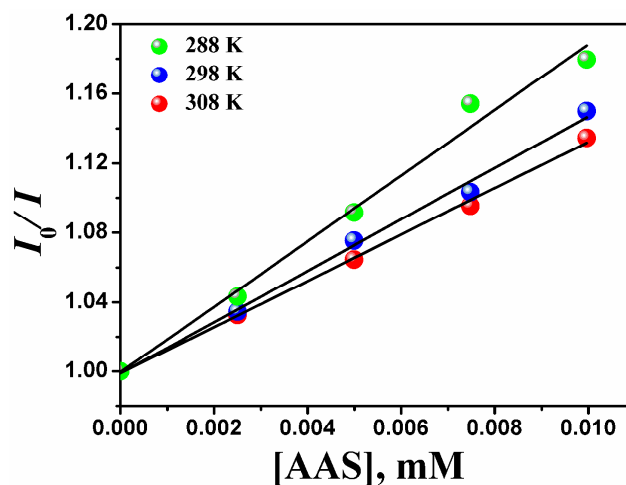

Fig. 6 Stern-Volmer quenching curves for BSA-AAS systems in region I at different temperatures, $[BSA] = 3.0$ μM.

Upon increment of AAS concentration beyond 0.015 mM the emission intensity (I) remains almost constant up to 0.56 mM AAS (Fig. 4) and the K_{SV} value in this region is found to be

quite low in comparison to the previous region 0.31 ($\pm$ 0.02) $\times$ 10^3 M^{-1} (at 298 K). The Scatchard plot for the region II is shown in Fig. S7. The negative ΔG_b° value indicates that the binding interaction between AAS and BSA is spontaneous in this region (Table S1). However, in region II, the emission maximum (λ_{em}) undergoes a further blue shift by 2 nm, indicating the fluorophores experience a more hydrophobic environment than in the previous region (Fig. 3 inset). This clearly indicates a further change in conformation of BSA, at the same time the small value of *n* (Table 2) suggests that the tendency of AAS to bind to BSA is low enough in this region which is presumably because of steric factor since AAS is flanked by two hydrophobic moieties on either side of the amide bond.

Table 2: Binding parameters from Scatchard plot of BSA-AAS system

Region	$10^3 \times K$, M^{-1}	n
I	1.11 $\pm$ 0.02	4.01 $\pm$ 0.03
II	2.23 $\pm$ 1.15	7.75 $\pm$ 1.22
III	128.34 $\pm$ 2.02	27.58 $\pm$ 1.82

After region II, the added surfactant molecules start to form micelle-like aggregates which are evident by the break observed at the end of this region (Fig. 4). This is in consistent with the tensiometric results where the local aggregation of AAS commences at around 0.54 mM (Fig. 1). The value of K and n also increases in this region as a result of micellization of AAS monomers (Table 2). Fig. 5S b shows the Stern-Volmer plot in region III and the K_{SV} value (1.63 $\pm$ ($\pm$ 0.07) $\times$ 10^3 M^{-1} at 298 K) is found to be significantly high as compared to region II (Table S1). The Scatchard plot for region III with negative cooperative nature is shown in Fig. S8. The sharp decrease in fluorescence intensity suggests substantial unfolding of the protein structure exposing the Trp residues towards the more hydrophilic environment. The emission maxima show a 3 nm red shift indicating that the micro environment near the Trp

residues is more polar as compared to that in the previous region. From the K value (Table 2), it can be inferred that the binding of AAS to BSA is strong enough and even much stronger than in region I. The high magnitude of n also suggests that the binding affinity of AAS toward BSA is highest in region III (Table 2). The region IV is rather a saturation phase where the added AAS does not show any affinity toward BSA. Therefore, the emission maxima (Fig. 3 inset) and emission intensity (Fig. 3) do not undergo any significant change during this region.

3.4. Time-resolved fluorescence decay studies

Intrinsic fluorescence life-time measurement serves as a promising tool to explore the conformational dynamics of a protein, and it is sensitive to excited state interactions [54]. In our present work, the amendment of Trp life-time upon stepwise addition of AAS has been investigated and the representative decay profile is shown in Fig. 7. From Fig. 7, it is clear that the added AAS molecules reduce the life-time of BSA caused by unfolding of the protein structure. The Trp emission has been fitted to a bi-exponential decay, and the deconvoluted data are summarised in Table 3. Although it is quite difficult to assign the contribution of the individual components to the average life-time in a multi-exponential decay, we have taken an attempt to shed some light on the variation of the relative amplitudes of the two components of BSA upon stepwise addition of AAS.
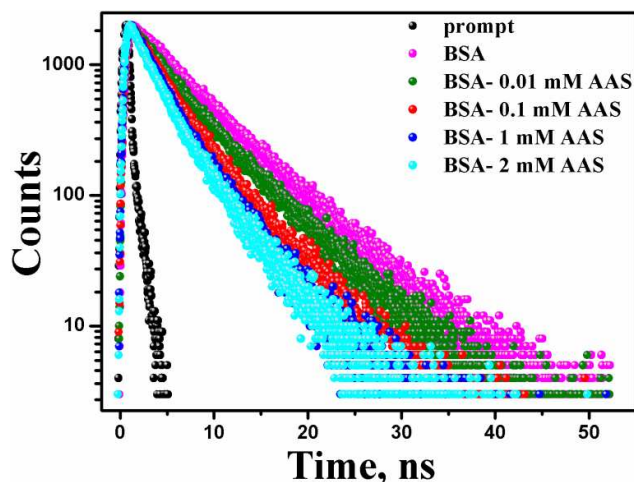
Fig. 7: Fluorescence life-time decay of BSA in the absence and presence of AAS at 298 K, [BSA] = 3.0 μM

It is well reported in literature that Trp-213 of BSA (like Trp-214 of HSA) is surrounded by a number of lysine residues [55]. A recent study by Chen *et al* reveals that lysine side chains quench 3-methylindole (a representable model of Trp) fluorescence via excited state proton transfer [56]. Thus in our present study, shorter life-time (τ_1), 3.79 ns has been assigned to Trp-213, buried in the hydrophobic core of protein, while the longer life-time (τ_2), 6.93 ns is due to the solvent-exposed residue, Trp-134 [57-60]. In Table 3, the values of pre-exponential factors ($a_2 < a_1$) indicates that the dominant contribution to the Trp life-time arise from Trp-134 residue. To understand the mode of unfolding of BSA induced by the added AAS molecules, we have plotted the average life-time ($\langle\tau\rangle$) of BSA against AAS concentration using Eq. 13, as shown in Fig. 8.

$$\log\left\{\frac{(\langle\tau_0\rangle-\langle\tau\rangle)}{\langle\tau\rangle}\right\}=\log\left\{\frac{K}{M^{-n}}\right\}+n\log\left\{\frac{[Q]}{M}\right\} \qquad (13)$$

where, $\langle\tau_0\rangle$ and $\langle\tau\rangle$ are the average life-time of BSA in the absence and presence of AAS. $[Q]$

is the concentration of quencher, here it is AAS. Fig. 8 implies that $\langle\tau\rangle$ changes in a stepwise

fashion in the presence of AAS, consistent with the sequential unfolding of BSA in Fig. 4.

Table 3. Fluorescence decay parameters of BSA in the absence and presence of AAS.

[AAS], mM	a_1	τ_1, ns	a_2	τ_2, ns	$\langle\tau\rangle^a$, ns	$\chi^{2\,b}$
0	0.38	3.79	0.62	6.93	5.72	1.09
0.006	0.44	3.24	0.56	6.49	5.08	1.09
0.02	0.53	2.99	0.47	5.92	4.37	1.03
0.04	0.57	2.55	0.43	5.48	3.92	1.08
0.06	0.60	2.67	0.40	5.53	3.79	1.02
0.12	0.61	2.74	0.39	5.61	3.72	1.07
0.6	0.63	2.89	0.37	5.57	3.70	1.03
1.2	0.66	2.08	0.34	4.62	2.94	1.05
2.0	0.68	2.03	0.32	4.64	2.85	1.07

$^a\langle\tau\rangle$ values have been calculated using Eq 2. ^{b} The magnitude of χ^2 indicates the goodness of fitting.

Four distinct regions (I – IV) are identified in Fig. 8. In region I, life-time of BSA changes

from 5.72 ns (native state) to 3.8 ns. From Table 3, it is observed that the contribution from

Trp-213 residue changes from about 38% to about 60%, and that for Trp-134 residue from

about 62% to about 40%. It implies that the buried Trp-213 exposes to the solvent whereas

the Trp-134 is pushed to a less polar environment caused by the unfolding of BSA even in

low concentration region of AAS. This observation is in line with the steady-state

fluorescence results as discussed previously from Fig. 4. In the later region (region II), $\langle\tau\rangle$

remains approximately constant (3.79 ns to 3.71 ns) over an appreciable range of AAS

concentration up to 0.58 mM. In this region, the tendency of AAS to bind to BSA is low

enough due to steric factor as we have stated previously. Beyond 0.58 mM AAS, micelle-like

aggregates start to form. Thus during the region III, protein-surfactant assembly swells in size, and Trp 213 experiences a more polar environment than in the previous region [61]. As a result, the relative amplitude of Trp-213 increases to about 66%. In this region, the value of ⟨τ⟩ decreases to 2.94 ns at 1.2 mM AAS indicating unfolding of the secondary structure of BSA and the type of binding of AAS to BSA in region III is assigned to be negative cooperative in nature. In the later region (region IV), the value of ⟨τ⟩ remains almost unchanged implying the binding process to be reached to the completion, and this result is also in consistent to our previous observation (Fig. 4)
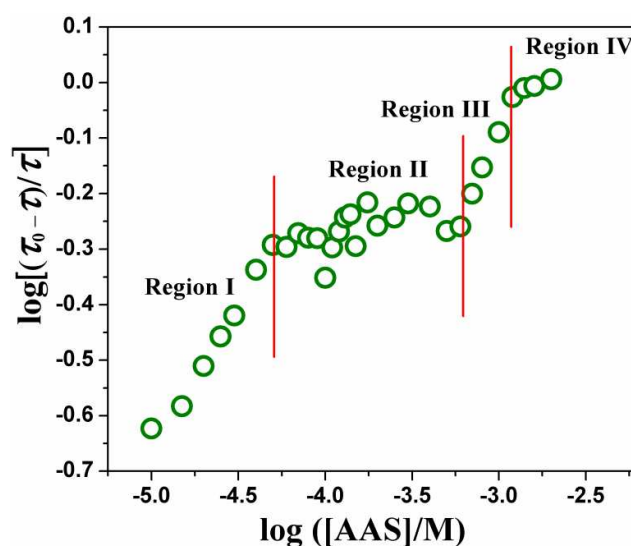

Fig. 8: Plot of $\log[(\tau_0-\tau)/\tau]$ *versus* $\log\{[AAS]/M\}$ representing various stage of binding of AAS to BSA at [BSA] = 3.0 μM, 298 K and pH 7.4.

3.6. Circular dichroism measurements

Circular dichroism (CD) is a widely applied and powerful technique used to explore the conformational alteration of the secondary structure of protein induced by surfactants [62]. Fig. 9 shows the far-UV CD spectra of native BSA in the absence and presence of the surfactant investigated. It is worth to note here that the surfactant, AAS does not contribute to

the CD spectra in the wavelength range of 200-260 nm. Hence the CD spectra, as we observe in Fig. 9, are solely contributed by BSA, and characterised by two negative bands at 208 nm and 220 nm due to $\pi \rightarrow \pi^*$ and $n \rightarrow \pi^*$ transition in the peptide bonds of α-helix respectively [63]. The changes of α-helical structure of BSA is used to ascribe qualitatively by the amendment in the ellipticity at 222 nm ($-\theta_{222}$). From Fig. 9, it is found that $-\theta_{222}$ decreases in a stepwise manner upon gradual addition of AAS. In our present work, the CD measurements have been carried out using BSA concentration of 1.5×10^{-7} M (as mentioned in the experimental section), whereas the AAS concentration has been kept same to that used in the previous experiments. Thus there will hardly be any such correspondence between the data obtained from CD spectra and that from previous techniques.
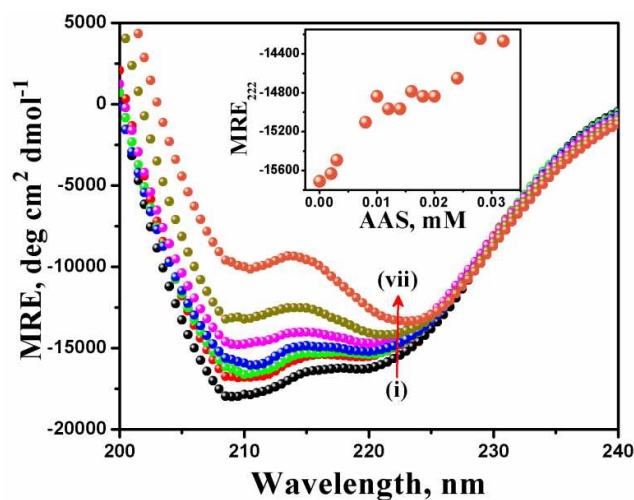

Fig. 9: CD spectra of BSA in the presence of AAS, (i)→(vii) correspond to 0, 1.0, 2.0, 4.0, 8.0, 16.0 and 32.0 μM AAS at [BSA] = 0.15 μM, 298 K and pH 7.4. Inset: variation of MRE at 222 nm against various AAS concentration at 298 K.

The secondary structural contents of BSA have been calculated employing a computer based programme, CDNN analysis. The α-helical content of BSA in the absence of AAS is obtained

to about 64% which is in consistent with the literature report [64]. In deciphering the effect of added AAS molecules on the secondary structure of BSA, we have plotted the MRE data at 222 nm (calculated using Eq. 3) *versus* AAS concentration, and the graph is shown as inset of Fig. 9. Upon successive addition of AAS, the content of α-helix decreases considerably while that of β-sheets, β-turn and random coil increases to the different extents (Table S3). It is observed that at low molar ratio of AAS to BSA ([AAS]/[BSA]) of 20, the α-helical content decreases to about 58% implying initial unfolding of the protein. Mukherjee *et al* recently reported that SDS stabilises BSA in low concentration region of the surfactant [25]. However, our present surfactant, AAS contains amide linkage forming H-bond with amino acid residue of BSA. Thus AAS binds tightly with BSA causing unfolding of the secondary structure even in the low concentration range. At higher AAS concentration, the content of α-helix undergoes drastic diminution to about 38% at a ratio of 200, which is ascribed due to AAS-aggregate induced unfolding. From Fig. 9, it is evident that the $-\theta_{222}$ peak undergoes an overall red shift by 3 nm, which is a signature of the possibility of hydrogen bonding in the system. Molecular docking study as will be discussed later also enlightens the fact of hydrogen bonding network between AAS and BSA.

3.7 Molecular docking studies

Molecular docking study has achieved an enormous attention in recent years in revealing the mode of binding of a small molecule relative to a macromolecular architecture. Recently, our research group has applied the molecular modeling in predicting the catalytic activity of cyclodextrins (α, β and γ) on the alkaline hydrolysis of malachite green [65]. However, the application of docking simulation in the case of binding of surfactant to various sites of a protein molecule is of burgeoning interests [66]. In our present work, the molecular simulation study has been accomplished to predict the binding regions offered by BSA to the

anionic surfactant (AAS) investigated. To substantiate the experimental results, 25 possible

docked conformations of the BSA-AAS complex have been modeled by AutoDock program

(as mentioned in the method section), out of which two conformations with negative binding

energies have been considered to be the best ranked results, and are shown in Fig. 10. The

binding energy of the most stable docked form (Fig. 10 (a)) is evaluated as – 3.44 kcal/mol.

The free energy change (ΔG_b°) for binding of AAS to BSA calculated experimentally is found

as –24.81 kJ/mol, and computed theoretically is –14.45 kJ/mol. The slight difference in the

above two energy values is due to the fact that the X-ray structure of BSA from crystal is

significantly different from that in the aqueous system used in our present study. This in

consequence offers different microenvironments to AAS to bind with BSA. The close-up

view of this docked form is shown in Fig. 10 (b) which reveals that AAS binds to sub domain

IIA, where Trp-213 is housed. Trp-213 and AAS is found to be much closer to each other,

and the measured distance between them is found as 4.31 Å, which is also in line with our

previous spectroscopic observation. Moreover, in domain II, AAS is surrounded by a number

of amino acid residues, namely, Trp-213, Tyr-451, Asp-450, Lys-294, Arg-194, Lys-221,

Arg-217 and Val-342 [67]. Thus there is a possibility of H-bonding interaction involving

carboxylate head group and amide moiety of AAS with those amino acid residues of BSA.

From docking study, it has been observed that the anionic head group, –COO⁻ of AAS forms

H-bond with –NH of Lys-294 showing a distance of 2.39 Å between them (Fig. 10 (b)). The

formation of a hydrogen bond with a bond length of 1.94 Å has been recognised between –

NH of Arg-217 and –COO⁻ of AAS. Another H-bond has also been traced between the –CO

in the amide (–C(O)NH) of AAS and –NH of Val-342 giving rise to a bond length of 2.01 Å.

H-bonding suggests a decrease in hydrophilicity, supporting well the blue shifting of λ_{em} of

Trp emission spectra in the presence of AAS (Fig. 3).

Another docked form of BSA-AAS complex have also been observed (Fig. 10 (c)) with binding energy somewhat less (–2.85 kcal/mol) than the former one. In this complex, AAS is found to bind in the sub domain IIIA mainly via H-bonding interaction. As investigated from the docking study (Fig. 10 (d)), the polar head group of AAS is exposed towards outside, while the hydrophobic tail is observed to be encompassed by a number of amino acid residues, namely, Lys-431, Arg-427, Ser-428, Glu-424, Arg-458 and Tyr 451. A hydrogen bond is found to be formed with the bond length of 2.59 Å between–CO of Glu-424 and–NH in –C(O)NH moiety of AAS. Another H-bonding interaction is identified between –NH of Arg-458 and –CO in the amide moiety of AAS with the bond length of 2.69 Å. Thus the docking simulation studies indicate the presence of a strong interaction between BSA and AAS, and it is also in line with the results already gathered by the previous techniques.
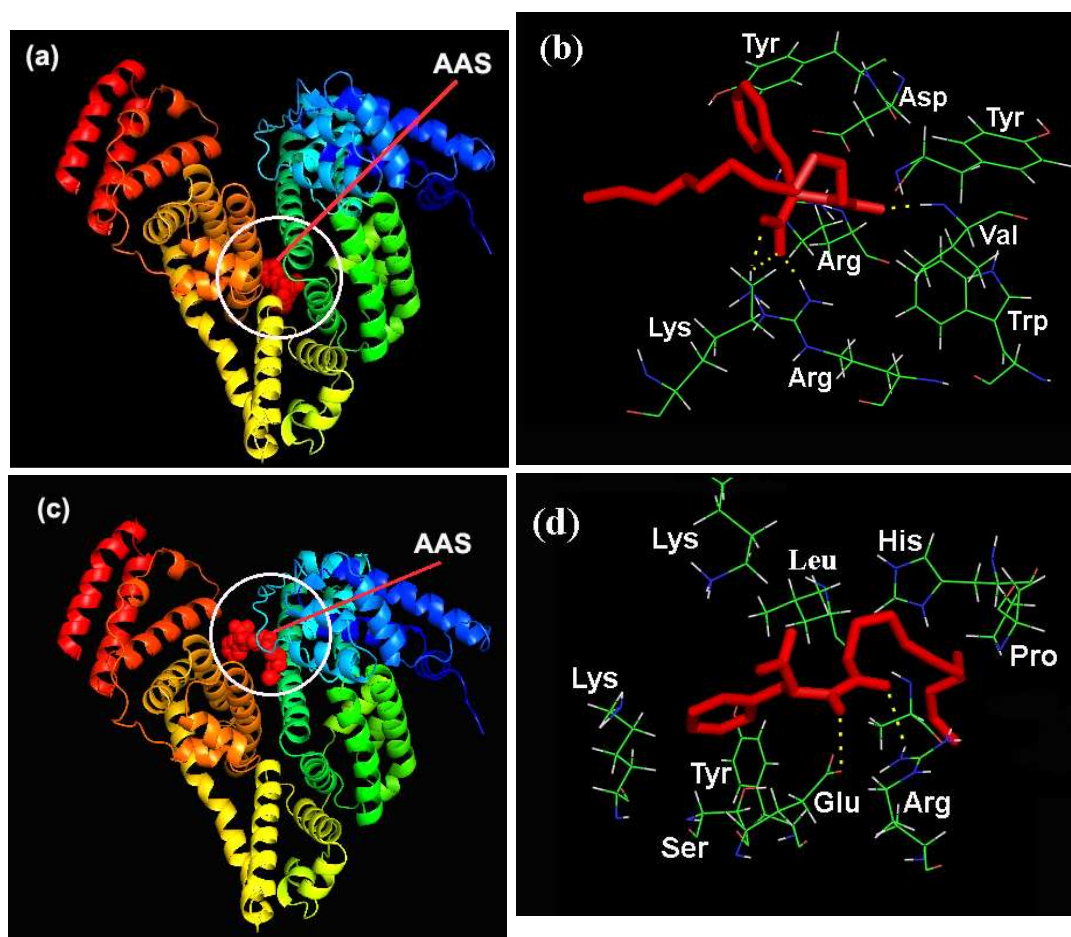
Fig. 10: (a) & (c) are the lowest energy binding modes of AAS to BSA. Secondary structure of BSA is displayed by ribbon and tube, and AAS is displayed by space ball and coloured in dark red. (b) & (d) are close-up views of binding sites of AAS on BSA corresponding to (a) & (c) respectively where AAS has been shown by stick model (red coloured) and the selected amino acid residues are shown by line model with colour variants as: CHNO

Possible bonding interactions are shown in yellow dotted line.

4. Conclusion

A number of methods have been applied to investigate the interactive phenomenon between the anionic surfactant, AAS and transport protein, BSA at physiological pH. The cmc of AAS shifts to higher value, 0.54 ($\pm$ 0.01) mM, in the presence of BSA as compared to that in the aqueous buffer medium, 0.31 ($\pm$ 0.02) mM, indicating significant interaction between them. The increase of negative ξ-potential value of the protein upon the addition of AAS indicates that the dominant interaction is non-columbic in nature. Steady-state fluorescence and life-time measurements reveal four characteristic binding regions. Scatchard plot of fluorescence data suggests that the binding is mainly negative cooperative in nature with non-identical and dependent set of binding sites. In region I, the monomeric binding of AAS to high affinity sites of BSA have been deciphered by molecular docking analysis which indicates that the surfactant approaches to the hydrophobic binding site of the protein i.e., sub domain IIA where Trp-213 is housed, and thereby influences the intrinsic fluorescence of BSA. Despite this docked form, AAS also docks in sub domain IIIA causing a change in protein conformation. Extensive H-bonding interactions have been observed in both of the docked forms involving the amide linkage present in the surfactant structure. In the later regions, AAS binds to BSA in the form of smaller aggregates and micelles resulting further unfolding of the protein structure. The CD experiments show the gradual depletion of α-helical

structure of BSA in the presence of AAS. Keeping in mind the 76% sequence homology between BSA and HSA, the present work is expected to provide an important insight into the interaction of the serum proteins with the anionic biocompatible amino acid surfactants.

Acknowledgements

References

1. F. L. Cui, J. Fan, J. P. Li and Z. D. Hu, *Bioorg. Med. Chem*. 2004, **12**, 151–157.

2. T. Peters, *"All About Albumin: Biochemistry, Genetics, and Medical Applications"*, Academic: San Diego, 1996.

3. A. Sulkowska, B. Bojko, J. Rownicka and W. Sulkowski, *J. Mol. Struct*., 2003, **651**, 237−243.

4. J. W. Smalley, P. Charalabou, C. A. Hart and J. Silver, *Microbiology*, 2003, **149**, 843−853.

5. E. D. Goddard and K. P. Ananthapadmanabhan, "*Interactions of surfactants with polymers and proteins"*, CRC Press Inc.: London, 1992.

6. M. Wilcox, *In Poucher's perfumes, cosmetics and soaps*, 10th ed.; Butler, H., Ed.; Kluwer Academic Publishers: Dordrecht, The Netherlands, 2000; pp 453−465.

7. M. N. Jones, *Chem. Soc. Rev.*, 1992, **21**, 127−136.

8. D. J. McClements, "*Food Emulsions: Principles, Practice, and Techniques*"; CRC Press: Boca Raton, FL, 2004.

9. G. Prieto, J. Sabín, J. M. Ruso, A. González-Pérez and F. Sarmiento, *Colloids Surf. A: Physicochem. Eng. Aspects*, 2004, **249**, 51–55.

10. C. Giancola, C. D. Sena, D. Fessas, G. Graziano and G. Barone, *Int. J. Biol. Macromol.*, 1997, **20**, 193−204.

11. B. X. Huang, H. Y. Kim and C. Dass, *J. Am. Soc. Mass Spectrom.*, 2004, **15**, 1237−1247.

12. P. Hazra, D. Chakrabarty, A. Chakraborty and N. Sarkar, *Biochem. Biophys. Res. Commun.*, 2004, **314**, 543-549.

13. (a) Y. Moriyama and K. Takeda, *Langmuir*, 1999, **15**, 2003-2008. (b) Y. Moriyama and K. Takeda, *Langmuir*, 2005, **21**, 5524-5528. (c) Y. Moriyama, E. Watanabe, K. Kobayashi, H. Harano, E. Inui and K. Takeda, *J. Phys. Chem. B*, 2008, **112**, 16585-16589. (d) Y. Moriyama, Y. Sato and K. Takeda, *J. Colloid Interface Sci.*, 1993, **156**, 420−424.

14. M. A. Mir, M. Gull, J. M. Khan, R. H. Khan, A. A. Dar and G. M. Rather, *J. Phys. Chem. B*, 2010, **114**, 3197-3210. (b) K. Sahu, S. K. Mondal, D. Roy, R. Karmakar and K. Bhattacharyya, *Chem. Phys. Lett.*, 2005, **413**, 484-489.

15. S. S. Krishnakumar, Panda, D. *Biochemistry* 2002, 41, 7443-7452.

16. M. D. Charbonneau and H. A. T. Richie, *J. Phys. Chem. B*, 2010, **114**, 1148–1155.

17. (a) E. L. Gelamo, R. Itri, A. Alonso, J. V. da Silva and M. Tabak, *J. Colloid Interface Sci.*, 2004, **277**, 471−482. (b) D. Kelley and D. J. McClements, *Food Hydrocolloids* 2003, **17**, 73−85.

18. D. Wu, G. Xu, Y. Sun, H. Zhang, H. Mao and Y. Feng, *Biomacromolecules*, 2007, **8**, 708−712.

19. V. I. Martin, A. Rodriguez, A. Maestre, and M. L. Moya, *Langmuir* 2013, **29**, 7629−7641.

20. D. E. Otzen, *Biochim. Bio-phys. Acta*, 2011, **1814**, 562–591.

21. A. Stenstam, A. Khan, and H. Wennerstrom, *Langmuir*, 2002, **17**, 7513–7520.

22. C. M. Dobson, *Biochem. Sci.*, 1999, **24**, 329.

23. N. P. Moore, S. Puvvada, D. Blankschtein, *Langmuir*, 2003, 19, 1009–1016.

24. (a) S. Shingawa, M. Sato, K. Kameyama and T. Takagi, *Langmuir* 1994, **10**, 1690-1694. (b) X. H. Guo, N. M. Zhao, S. H. Chen and J. Teixeira, *Biopolymers*, 1990, **29**, 335-346. (c) K. P. Ananthapadmanabhan, in: E.D. Goddard, K.P. Ananthapadmanabhan (Eds.), "*Interactions of Surfactants with Polymers and Proteins*", first ed., CRC Press, London, 1993, p. 319.

25. U. Anand and S. Mukherjee, *Phys. Chem. Chem. Phys.*, 2013, **15**, 9375-9383.

26. R. Kaur and R. K. Mahajan, *RSC Adv.*, 2014, **4**, 29450–29462.

27. M. R. Infante, A. Pinazo and J. Seguer, *Colloid Surf. A*, 1997, **123–124**, 49–70.

28. T. Peters (1975). Putman FW, ed. "*The Plasma Proteins*". Academic Press. pp. 133–181.

29. S. Miyagishi and M. Nishida, *J. Colloid Interface Sci.*, 1978, **65**, 380–386.

30. A. Kundu, S. Dasmandal, T. Majumdar and A. Mahapatra, *Colloids and Surfaces A: Physicochem. Eng. Aspects*, 2013, **419**, 216– 222.

31. J. R. Lakowicz, "*Principles of Fluorescence Spectroscopy*", Springer, US, 3rd edn, 2006.

32. A. Dan, I. Chakraborty, S. Ghosh and S. P. Moulik, *Langmuir* 2007, **23**, 7531-7538.

33. (a) M. van de Weert and L. Stella, *J. Mol. Struct.*, 2011, **998**, 144–150. (b) W. Zong, R. Liu, F. Sun, Y. Teng, Xiaoyan Fang and Jun Chai, *J. Fluoresc*, 2011, **21**, 1249–1254. (c) L. Stella, A. L. Capodilupo and M. Bietti, *Chem. Commun.*, 2008, 4744–4746.

34. H. M. Berman, J. Westbrook, Z. Feng, G. Gilliland, T. N. Bhat, H. Weissig, I. N. Shindyalov and P. E. Bourne, *Nucleic Acids Res.*, 2000, **28**, 235−242.

35. W. Khon and L. J. Sham, *Phys. Rev.*, 1965, **140**, A1133.

36. G. M. Morris, D. S. Goodsell, R. S. Halliday, R. Huey, W. E. Hart, R. K. Belew and A. J. Olson, *J. Comput. Chem.* 1998, **19**, 1639−1662.

37. W. L. De Lano, *The PyMOL Molecular Graphics System*, De Lano Scientific, San Carlos, CA, USA, 2004.

38. S. F. Santos, D. Zanette, H. Fischer and R. Itri, *J. Colloid Interface Sci.*, 2003, **262**, 400–408.

39. C. Das, T. Chakraborty, S. Ghosh and B. Das, *Colloid Polym. Sci.* 2008, **286**, 1143-1155.

40. T. Chakraborty, I. Chakraborty, S. P. Moulik and S. Ghosh, *Langmuir* 2009, **25**, 3062−3074.

41. S. Miyagishi, M. Takagi, S. Kadono, A. Ohta, and T. Asakawa, *J. Colloid Interface Sci.*, 2003, **261**,191−196.

42. J. Sabin, G. Prieto, A. Gonzalez-Perez, J. M. Ruso, and F. Sarmiento, *Biomacromolecules*, 2006, **7**, 176-182.

43. N. Miyake, T. Sato and Y. Maki, *Bull Tokyo Dent Coll*, 2013, **54**, 97-101.

44. E. L. Gelamo, C. H. Silva, H. Imasato and M. Tabak, *Biochim. Biophys. Acta*, 2002, **1594**, 84-99.

45. W. G. Liu, K. D. Yao, G. C. Wang and H. X. Li, *Polymer*, 2000, **41**, 7589−7592.

46. Y. Shu, M. Liu, S. Chen, X.-W. Chen and J.-H. Wang, *J. Phys. Chem. B*, 2011, **115**, 12306-12314.

47. S. Koutsopoulos, A. Tjeerdsma, J. F.T. Lieshout, J. van der Oost and W. Norde, *Biomacromolecules*, 2005, **6**, 1176–1184.

48. Y.J. Hu, Y. Liu, R.M. Zhao, J.X. Dong and S.S. Qu, *J. Photochem. Photobiol. A*, 2006, **179**, 324 – 329.

49. U. Anand, C. Jash and S. Mukherjee, *J. Phys. Chem. B.*, 2010, **114**, 15839-15845.

50. G. Ercolani, *J. Am. Chem. Soc.*, 2003, **25**, 16097–16103.

51. F. Karush and M. Sonenberg, *J. Am. Chem. Soc.*, 1949, **71**, 1369-1376.

52. P. D. Ross and S. Subramanian, *Biochemistry*-US 1981, **20**, 3096–3102.

53. J. A. Lefstin and K. R. Yamamoto, *Nature*, 1998, **392**, 885–888.

54. S. Matzinger, D. M. Hussey and M. D. Fayer, *J. Phys. Chem. B*, 1998, **102**, 7216−7224.

55. P. F. Spahr and John T. Edsall, *J. biol. Chem.*, 1964, **239**, 850-854.

56. Y. Chen and M. D. Barkley, *Biochemistry*. 1998, **37**, 9976–9982.

57. A. Grinvald and I. Z. Steinberg, *Biochim. Biophys. Acta*, 1976, **427**, 663–668.

58. J. Tiana, Y. Zhaob, X. Liua and S. Zhaoa, *Luminescence*, 2009, **24**, 386–393.

59. S. De, A. Girigoswami and S. Das, *J. Colloid and Interface Science* 2005, **285**, 562–573.

60. Min Li and Ann E. Hagerman, *J. Agric. Food Chem*. 2014, **62**, 3768−3775.

61. K. Takeda and K. Yamamoto, *J. Protein Chem.* 1990, **9**, 17-22.

62. N. Sreerama and R. W. Woody, *Anal. Biochem.*, 2000, **287**, 252−260.

63. Yang, P.; Gao, F. "*The Principle of Bioinorganic Chemistry*", Science Press: Beijing, China, 2002; p. 349.

64. P. Bharmoria, K. S. Rao, T. J. Trivedi, and A. Kumar, *J. Phys. Chem. B*, 2014, **118**, 115−124.

65. S. Dasmandal, H. K. Mandal, S. Rudra, A. Kundu, T. Majumdar and A. Mahapatra, *RSC Adv.*, 2015, **5**, 38503-38512.

66. Y. S. Ge, S. X. Tai, Z. Q. Xu, L. Lai, F. F. Tian, D. W. Li, F. L. Jiang, Y. Liu, and Z. N. Gao, *Langmuir*, 2012, **28**, 5913−5920.

67. A. S. Sharma, S. Anandakumar and M. Ilanchelian, *J. Lumin.*, 2014, **151**, 206-218.